Current Osteoporosis Reports (2018) 16:77–94
https://doi.org/10.1007/s11914-018-0421-4

GENETICS (M JOHNSON AND S RALSTON, SECTION EDITORS)

Screening Gene Knockout Mice for Variation in Bone Mass: Analysis by μCT and Histomorphometry

David W. Rowe[1] · Douglas J. Adams[2] · Seung-Hyun Hong[3] · Caibin Zhang[1] · Dong-Guk Shin[3] · C. Renata Rydzik[2] · Li Chen[1] · Zhihua Wu[1] · Gaven Garland[4] · Dana A. Godfrey[5] · John P. Sundberg[4] · Cheryl Ackert-Bicknell[5]

Published online: 5 March 2018

Abstract

Purpose of review The international mouse phenotyping consortium (IMPC) is producing defined gene knockout mouse lines. Here, a phenotyping program is presented that is based on micro-computed tomography (μCT) assessment of distal femur and vertebra. Lines with significant variation undergo a computer-based bone histomorphometric analysis.

Recent findings Of the 220 lines examined to date, approximately 15% have a significant variation (high or low) by μCT, most of which are not identified by the IMPC screen. Significant dimorphism between the sexes and bone compartments adds to the complexity of the skeletal findings. The μCT information that is posted at www.bonebase.org can group KOMP lines with similar morphological features. The histological data is presented in a graphic form that associates the cellular features with a specific anatomic group.

Summary The web portal presents a bone-centric view appropriate for the skeletal biologist/clinician to organize and understand the large number of genes that can influence skeletal health. Cataloging the relative severity of each variant is the first step towards compiling the dataset necessary to appreciate the full polygenic basis of degenerative bone disease.

Keywords IMPC and KOMP · Bone phenotyping · μCT · Histomorphometry · Web portal

Research reported in this publication was supported by the National Institute of Arthritis and Musculoskeletal and Skin Diseases of the National Institutes of Health under Award Number R01 AR063702. The content is solely the responsibility of the authors and does not necessarily represent the official views of the National Institutes of Health."

This article is part of the Topical Collection on *Genetics*

Electronic supplementary material The online version of this article (https://doi.org/10.1007/s11914-018-0421-4) contains supplementary material, which is available to authorized users.

✉ David W. Rowe
drowe@uchc.edu

[1] Regenerative Medicine and Skeletal Development, Department of Reconstructive Sciences, Biomaterials and Skeletal Development, School of Dental Medicine, University of Connecticut Health, Farmington, CT 06030, USA

[2] Department of Orthopaedic Surgery, School of Medicine, University of Connecticut Health, Farmington, CT 06030, USA

[3] Computer Science and Engineering, School of Engineering, University of Connecticut, Storrs, CT 06269, USA

[4] The Jackson Laboratory, Bar Harbor, ME 04609, USA

[5] Center for Musculoskeletal Research, Department of Orthopaedics and Rehabilitation, University of Rochester School of Medicine, Rochester, NY 14642, USA

Introduction

Degenerative disorders of the skeleton, which include osteoporosis, comprise the second most costly disease category accounting for ~ 5.0% of the nation's GDP and by far exceed other categories for limiting the activities of daily living [1]. Because expensive pharmacologic and surgical interventions of the affected adult are at best palliative, the optimal strategy to reduce the financial and personal cost of this disease category is prevention [2]. However, the insidious onset and complex polygenetic nature of skeletal disease pose a challenge to a behavioral or pharmaceutical approach for prevention [3•]. For example, the largest GWAS to date for bone mineral density (BMD) suggests over 300 loci for this phenotype [4] and still only captures a fraction of the known heritability for this phenotype. A search for just the term "musculoskeletal abnormalities" yields 5234 entries in OMIM, most of which are orphans in that the disease-causing gene(s) remains unknown. There are over 500 known Mendelian diseases described in the literature that impact bones and joints, including 372 defined skeletal dysplasias wherein the skeleton is the primary organ system impacted by the disease-causing mutation [5]. The 13th publication of nosology of skeletal dysplasias now recognizes 436 distinct clinical disorders of which 89 are a monogenic disorder primarily affecting bone [6]. While anabolic and anti-resorptive acting pharmaceuticals exist to treat low bone mass, these drugs are ineffective in some patients, have serious side effects in others [7, 8], and in the case of anabolic drugs are contraindicated for children [9]. This spectrum of response reflects the genetic heterogeneity of disease affecting the skeleton [10]. Thus, identifying the genes that contribute to or protect against degenerative bone disease is the first step for a personalized behavioral or pharmaceutical intervention [11] prior to the onset of symptoms.

The number of publications that identify bone genes using global and targeted gene knockout mice is increasing exponentially. In many cases, these experiments were performed on mice with a variety of genetic backgrounds and used different molecular mechanisms for gene inactivation, and with inconsistent rigor of the analytical methods. While this literature underscores the broad range of genes that affect bone formation and maintenance, the inconsistency of method and analysis renders the relevance of the findings to human disease difficult to interpret. A number of unbiased high throughput screens of gene knockout mice have been performed to identify new genes causing skeletal disease. Lexicon screened 3255 mouse transgenic knockout (KO) lines using whole-body dual X-ray absorptiometry (DXA) and micro-computed tomography (μCT) of the femur and spine. They reported on 23 known and 13 previously unappreciated bone disorders [12]. Other screens by Genentech and Wellcome Trust Sanger Institute respectively showed that between 32 and 6% of KO lines have identifiable bone phenotypes [13, 14]. A similar outcome is being obtained from the International Mouse Phenotyping Consortium (IMPC) in European studies [15, 16•]. Estimates calculated using our own data from phenotyping IMPC-derived mice suggests that 2000–2400 genes will have a significant bone mass variance that would render an individual either more or less susceptible to bone fragility with advancing age. Thus, identifying the full spectrum of genes affecting bone mass will be a huge challenge, requiring the use of principles that have been successful in other "big data" programs.

By developing a genetic resource of well-defined mouse KO lines all on the same genetic background, the IMPC and its US component, the knockout mouse project (KOMP, https://www.genome.gov/17515708/), are providing one of the essential elements for a big data program for skeletal variation [17•]. These KOs are being analyzed for a broad spectrum of morphologic, metabolic, hematologic, and immune features that are searchable on their web portal (http://www.mousephenotype.org). Our goal is to utilize this foundation to build and test the elements of a large dataset that might have value for appreciating the spectrum of skeletal variation found in the mice. Four components of this analysis are presented here, which distinguish our approach from other phenotyping programs. First, we developed a screening protocol based on μCT as the most discriminatory tool for identification of a KO line with an interpretable phenotype. The primary musculoskeletal screening tool of the IMPC web portal is whole-body DXA, from which the bone mineral content (BMC) data are measured to identify mice with a skeletal mass phenotype. Whole-body BMC in rodents lacks the sensitivity for distinguishing cortical and trabecular components of bone despite increasing evidence showing that these bone compartments are independently genetically regulated [18, 19]. Second, we have incorporated measurement of bone and body size to recognize phenotypic categories of frailty and fitness, which are recognized phenotypes in human subjects. Third, a computer-automated dynamic and cellular histomorphology protocol [20, 21] has been applied to KO lines with significant variation in trabecular and cortical bone size to appreciate potential cellular mechanisms that might account for these phenotypic outliers. Fourth, the μCT and histomorphometric data are presented on a searchable web portal to allow the viewer to observe the primary data that underlies the conclusions. The ultimate goal of the web portal is to present sufficient information on a specific KO line to encourage the skeletal investigator to obtain the KOMP line for more detailed analysis.

Method

A more comprehensive description of the methods used to produce and analyze the KOMP mice and to understand its

presentation within the web portal (www.bonebase.org) will be published elsewhere. This information is abbreviated here to allow sufficient understanding of how the workflow was organized, performed, interpreted, and presented.

Laboratory Information Management System

A server-based database (Filemaker) was developed to manage all the workflow steps from the initial identification of a KOMP line to the final deposition of skeletal data that was posted on the web portal. Every sample at every step had a unique bar-code and readable label that was computer generated. The staff that processed the workflow recorded the completion of their process in the database including comments that might affect the outcome of the analysis.

Mouse Production and Tissue Collection

Homozygous KOMP breeder pairs were purchased from the ongoing KOMP phenotyping program at the Jackson Laboratory. Over the 4 years of the program, 220 KOMP lines proved to have sufficient fecundity to produce 8 male (M) and 8 female (F) offspring that could be grown to 12 weeks of age. C57BL/6NJ breeder controls were maintained concurrently to the knockout lines to produce 8 M and 8 F per month. At 11 weeks of age, the progeny were weighed and injected with calcein (6 mg/kg) and alizarin complexone (30 mg/kg) at 7 and 2 days respectively prior to sacrifice. The dissected tissues were placed in 10% cold formalin, packaged in wet ice, and sent to UCONN Farmington. Upon arrival, the samples were processed and held for μCT (femur and vertebra L1–3 using 70% ethanol at 4 °C) and histology (femur and L4-L6 using 30% sucrose at − 80 °C) until the full set of 8M and 8F were collected after which the KOMP line was terminated.

Micro-computed Tomography

When the full set of eight males and eight females constituting a KOMP line were received, the dissected femur and lower lumbar vertebrae (L4–L6) were processed as a sample set. Using the 10-carousel robotic feature of the scanner (μCT40, Scanco Medical) along with custom cruciform-shaped specimen holder inserts (three tiers, four quadrants per tier), individual specimens were placed into the resulting defined locations using dental wax and imaged in 70% ETOH at 16 μm resolution (244,140 voxels per cubic millimeter). A de novo batch script was developed to scan these predefined specimen locations, further obviating the operator from the process. Image files for each specimen were reconstructed individually, carrying each unique identifying specimen number. For the femur, the operator identified the three transverse sections (image slices) at the proximal aspect of the femoral head, distal aspect of the femoral condyles, and center of the growth plate. From these locations, the remainder of the computational process was entirely automated, scaling selection of the mid-diaphyseal region of interest (ROI) defining cortical bone, and distal metaphysis ROI defining trabecular compartment, to femur length measured from the femoral head to the condyles. All anatomical boundaries and computation of morphometry were automated, exporting data in a format for visual inspection prior to uploading into the Laboratory Information Management System (LIMS) system. The trabecular ROI was placed ~ 5% of length (~ 0.8 mm) from the distal growth plate and extended proximally ~ 6% (~ 1 mm). The cortical ROI was placed ~ 40% of length (~ 6 mm) from the distal growth plate and extended distally ~ 4% of length (~ 0.6 mm). Another custom script was developed for processing vertebrae to select the trabecular compartment within the vertebral centrum. The operator selected transverse locations ~ 10% of vertebral height within each endplate and placed a rectangular prism bounding the centrum. The volumetric ROI comprising the trabecular compartment of the centrum was found automatically using a series of shape transformations and all morphometric parameters calculated automatically, again exporting data for visual inspection and upload to the LIMS system. Although all standard morphometric parameters defining trabecular and cortical compartments were measured, the morphometric measurements that will be emphasized here are the bone volume fraction within the trabecular compartment (BV/TV) of the distal femur and L4 vertebra, the volume of the metaphyseal trabecular compartment as determined by the ROI within the distal femur (TV), and the total subperiosteal area (Tt.Ar) enveloping the femur at mid-diaphysis, which will be abbreviated here as total area (TA).

Dynamic and Cellular Histomorphometry

The decision to perform this analysis was dependent on the outcome of the μCT analysis. Samples with significant variation in either trabecular bone volume or cortical size as well as the monthly controls were processed for the histological analysis. The entire set of 8 M and 8 F femur or vertebra were processed together. Videos of the following steps can be viewed on the web portal, and additional applications are described elsewhere [21]. The samples were thawed from a frozen 30% sucrose storage solution, and four samples were immediately refrozen in a single disposable 24 × 24 × 5 base mold in a parallel orientation such that the anterior distal femur and the vertebral bodies faced the surface of mold. The frozen block was mounted with the cassette side up on the specimen object disc of a Leica CM3050-S research grade cryostat and oriented so that the disposable steel blade cut the four samples at the same level. The block was cut to the approximate midpoint such that three ~ 7 μ thick sections were obtained at 50 μ intervals surrounding the central vein of the femur or the widest diameter of the vertebral body. The

sections were captured using a tape transfer method (Cryofilm type IIC(10), Section Lab) previously described [20, 21] and temporarily adhered to plastic slides that were maintained at − 20 °C until the next processing step.

The 12 tapes containing 48 sections from a M and F sample set of long bone or vertebra were mount on 6 glass slides (2 tapes containing all 8 sections from one section level and one gender) using UV-activated adhesive (Norland Optical Adhesive, 61). From a suspension of red and green fluorescent beads (6 μ), a 1-μl drop was placed on the tissue section away from the region that would subsequently become the ROI for the histological analysis. After the drops evaporated, the UV adhesive was activated using a controlled UVB light source (Spectroline XLE-1000) for 3 rounds of 1 J each (4–5 min each). Immediately after the crosslinking step, the six slides were hydrated in PBS for 1 min, overlaid with a 0.3-mg/ml calcium blue solution for 10 min, and cover-slipped with 50% glycerol diluted in PBS. The slides were loaded into Axioscan Z1 that was controlled by the Zen software. The ROI of each tissue section on each slide was demarcated, and the limits of the focal distance were determined for the automated focusing feature. These settings were saved for the subsequent imaging steps.

The first imaging step was performed on the mineralized section to record the accumulated mineral (DAC and calcein blue) and the calcein (green) and alizarin complexone (red) mineralization lines. The fluorescent images were captured on a gray-scale camera and subsequently color-coded by the software. Once the scanning was completed, the slides were placed in PBS to remove the cover slip in preparation for the TRAP staining/imaging procedure used to identify cells in the osteoclast lineage. The slides are overlaid with the TRAP reaction buffer (pH 4.2) for 10 min, which removes the accumulated mineral and fluorescent mineral labels. The slides are then overlaid with the fluorescent substrate ELF97 for 5 min after which the slides are dried, exposed to a UVB light source (Spectroline XLE-1000) for 1 J each (4–5 min) and a second round at 0.5 J, and then cover-slipped using 30% glycerol in PBS. The slides are imaged for ELF fluorescence (yellow), and the red and green channels are used to capture the location of the fluorescent beads. The third round of scanning/imaging uses the endogenous alkaline phosphatase (AP) to identify cell in the osteoblast lineage. The coverslips are removed after the TRAP scanning and equilibrated in AP reaction buffer (pH 9.5) followed by incubation in the fast red substrate for 10 min. The slides are mounted 50% glycerol/1:1000 DAPI in PBS and scanned for fast red, DAPI, and green. In the final round, the slides are stained in toluidine blue, cover-slipped in 30% glycerol in water, and scanned using an open filter and color camera.

The digital output from each round of scanning produces a jpg file which is labeled using a format that identifies the sample (M, F, section level, image type). These files are batch loaded to the LIMS and to a server located in the Computer Science Department at UCONN Storrs. Using a 24-node computer cluster, an in-house developed algorithm processes the jpg files through a series of steps that include (a) vertical alignment of the three fluorescent rounds of imaging utilizing the fluorescent beads followed by the selection of the ROI; (b) background correction and thresholding of the fluorescent signals; and (c) projection of the fluorescent signals to the surface of the mineralized tissues from which the mineral, AP, and TRAP signals are expressed as a percentage of mineralized surface. Videos of these steps plus those used to generate the histomorphometric measurements are presented on the web portal.

From these analyses, the following measurements are generated and the results are deposited into the LIMS:

1. Static bone volume—The bone volume with the ROI (BV/TV) and trabecular thickness are measured directly while trabecular number is added as a calculated value.
2. Dynamic bone activity—This is based on the mineralization lines and follows the rules of traditional bone histomorphometry. The single- and double-labeled surfaces are measured to determine the bone-forming surfaces (MS/BS) and mineral appositional rate (MAR) from which the bone formation rate is calculated.
3. Osteoblast surfaces—In lieu of visually identifying cells on the bone surface, the AP fluorescent signals are used to identify cells in the osteoblast lineage. Our previous work has shown that bone surface cells that express a differentiated osteoblast-restricted GFP reporter and overlie a recently formed fluorescent mineralization line have the RNA profile of a fully differentiated osteoblast when isolated by flow cytometry [22, 23]. Because these cells also have a strong AP enzymatic activity, the fluorescent histology utilizes the fluorescent AP signal that overlays the fluorescent mineralization line to identify a bone surface containing active matrix-forming osteoblasts. In addition, a weaker AP signal that lies on the bone surface that is GFP reporter negative and does not have an underlying mineralization line is identified as a bone lining cell (non-forming bone surfaces).
4. Osteoclast surface—The TRAP stain identifies cells within the osteoclast lineage but does not discriminate between mono or multinucleated cells. This signal can be detected over bone surfaces that are devoid of a mineralization label (resorbing surfaces) or have a mineralization label (remodeling surface).
5. Remodeling unit—The analysis also detects focal areas in which AP, TRAP, and a mineralization line co-localize. We have defined this area as a remodeling unit because it shows the biological activity envisioned by the BFU identified morphologically using traditional histological methods [24, 25].

Statistical Analysis

The between-batch variation in all μCT and histomorphometric measurement was greater than anticipated for an inbred mouse strain, especially in the males. This is not a unique phenomena for this project, as a similar degree of batch-associated variation is evident in the DXA-derived BMC and other biological measurements captured by the IMPC as part of their phenotyping pipeline. A linear mixed model statistical test for an interaction between genotype and phenotype is especially useful for large-scale screening. It uses the Fisher exact test [26] to assess for a significant difference observed between the knockout and control group for each gender. By delineating batch in the model, we were able to account for and correct for this variation in both the controls and the experimental animals. Specifically, this was accomplished using the Phenstat package, which was developed by the IMPC for this purpose [27]. We have applied the same $P < 0.0001$ significance threshold as is used by the IMPC to account for multiple testing [17•]. Second, we implemented a test to control ratio threshold to further avoid type I statistical error. The selected threshold ratio resulted in a 25–30/35–45% low/high difference for femur BV/TV, a 20% difference for vertebral BV/TV, a 15% difference for total cortical perimeter area (TA) and femur trabecular compartment size (TV), and 13% body weight (Wt) measurements (see supplemental Fig. 1). The position of a specific KOMP line relative to the total control or KOMP population is presented on the web portal in frequency distribution graphics. Thus, this dual "certification" is designed to provide confidence that a bone phenotype of a specific KOMP line is worthy of further investigation. KOMP lines that met these criteria were "called" by the computer program to be low or high for a specific measurement, and this call is used by the database component of the web portal to select for specific KO lines that manifest the variant measurement.

Results

Influence of Body Weight on Bone Architectural Measurements

The data generated from examining the control and KOMP lines as a group revealed useful information regarding the influence of body weight on the architectural measurements obtained by μCT. Figure 1a plots the mean BV/TV femoral or vertebral measurement of the individual KOMP line or control group divided by the mean weight of all the control groups. It demonstrates the absence of a correlation between these two variables ($r^2 < 0.2$) and calls into question the use of body weight to correct the BV/TV measurement. However, Fig. 1b presents the relationship of bone size ratio, based on femoral bone total cortical area and total volume versus the body weight ratio and demonstrates a moderate correlation ($\sim r^2 > 0.5$) in both sexes. Because DXA primarily measures the cortical bone mass, a correction based on body size may be justified although the correction factor cannot be established from the information obtained for this study. These results are summarized in Table 1.

Results of the Primary Screen by Micro-Computed Tomography

Upon entering the database section of the web portal, a selection interface is presented in which specific bone architectural measurements (BV/TV of distal femur and vertebra, the TV and TA of the femur, and body weight) are expressed as a ratio of the test versus the corresponding control value for each KOMP line examined (Fig. 2a). The header of each measurement provides a check box to select for a measurement that was called to be either high or low. The criteria for making these calls are shown in Fig. 1 of the supplement. A query for a single measurement will produce all lines that had that abnormal value without consideration for other measurement. The list can be sorted for the progression within either compartment or sex by clicking the appropriate hyperlink. To visually appreciate the degree of variance of any specific KOMP line from the control and other KOMP lines, double click the gene name. The frequency distribution curve (Fig. 2b) for any of the primary measures can be selected from the tab at the top of the page in which the specific KOMP line is presented in a magenta column against the binned values of the control (brown column) and KOMP lines (green columns).

The initial query identifies 19 lines with a significant reduction in BV/TV in either bone compartment while 29 KOMP lines are found with a high BV/TV. Within these groups, there are many examples of sexual and site (axial vs appendicular) dimorphism. Table 2 demonstrates that a low BV/TV that was limited to the femur was found in four KOMP lines in females only, in one KOMP line in males only, but in no KOMP line was it present in both sexes. A low BV/TV limited to the vertebra was not encountered. Instead, both the femur and vertebra were low in three females only and four males only, and in two lines, it was low in both bone and sexes. A similar distribution was observed for a high BV/TV but with predominance in males. Within the measures of bone size (femur total volume and cortical bone area) and body weight, there was remarkable male bias of sexual dimorphism with only a minority of both sexes having the same finding. These findings underscore the need to examine both sites in both sexes to not miss recognizing genes that impact bone architecture and body size. The table also scores the number of KOMP lines in each grouping that were scored by the IMPC web portal to have abnormality in bone mineral content or in body composition.

a

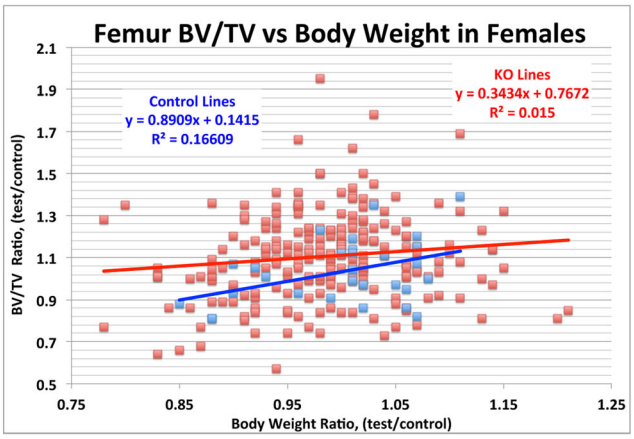
Femur BV/TV vs Body Weight in Females
Control Lines
y = 0.8909x + 0.1415
R² = 0.16609
KO Lines
y = 0.3434x + 0.7672
R² = 0.015
BV/TV Ratio, (test/control)
Body Weight Ratio, (test/control)

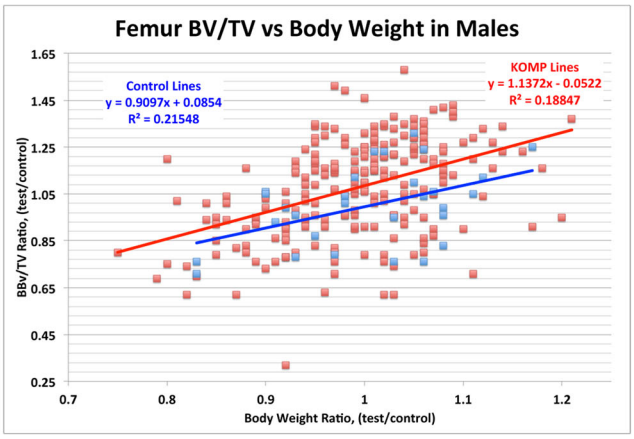
Femur BV/TV vs Body Weight in Males
Control Lines
y = 0.9097x + 0.0854
R² = 0.21548
KOMP Lines
y = 1.1372x - 0.0522
R² = 0.18847
BBv/TV Ratio, (test/control)
Body Weight Ratio, (test/control)

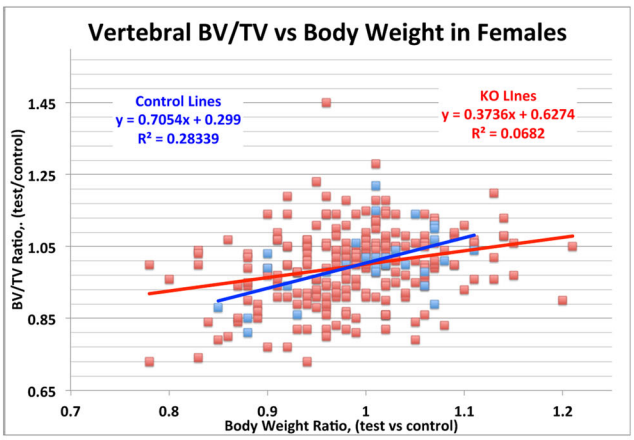
Vertebral BV/TV vs Body Weight in Females
Control Lines
y = 0.7054x + 0.299
R² = 0.28339
KO LIne
y = 0.3736x + 0.6274
R² = 0.0682
BV/TV Ratio,. (test/control)
Body Weight Ratio, (test vs control)

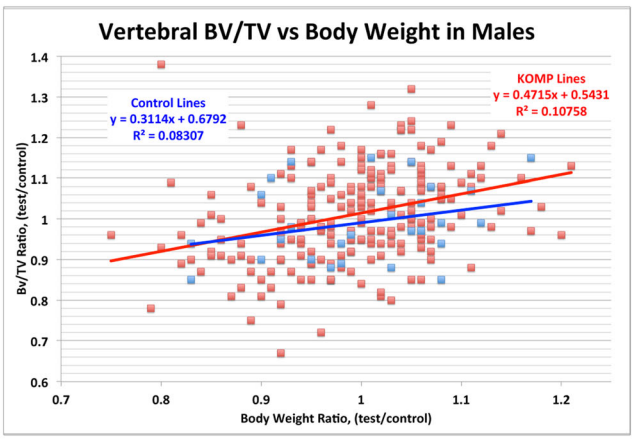
Vertebral BV/TV vs Body Weight in Males
Control Lines
y = 0.3114x + 0.6792
R² = 0.08307
KOMP Lines
y = 0.4715x + 0.5431
R² = 0.10758
Bv/TV Ratio, (test/control)
Body Weight Ratio, (test/control)

b

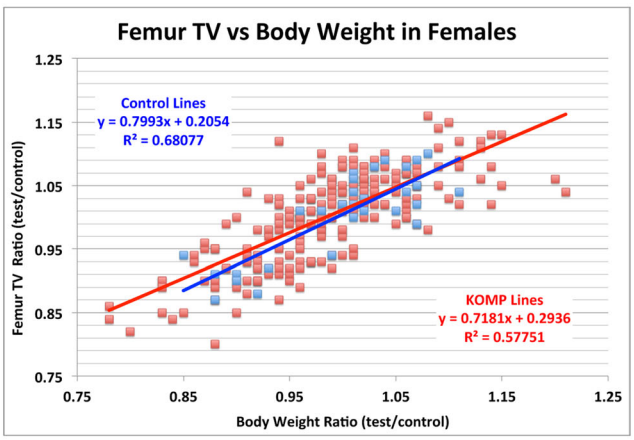
Femur TV vs Body Weight in Females
Control Lines
y = 0.7993x + 0.2054
R² = 0.68077
KOMP Lines
y = 0.7181x + 0.2936
R² = 0.57751
Femur TV Ratio (test/control)
Body Weight Ratio (test/control)

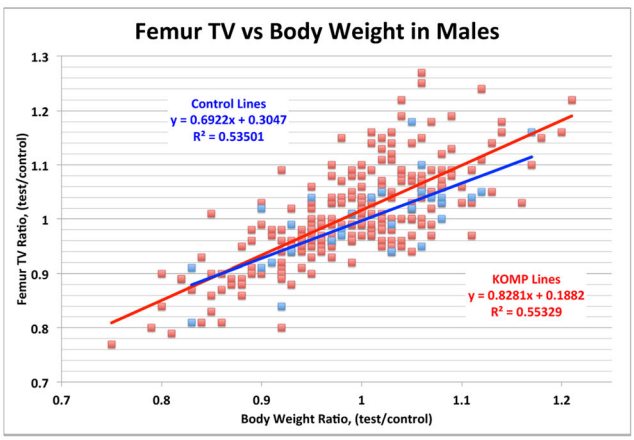
Femur TV vs Body Weight in Males
Control Lines
y = 0.6922x + 0.3047
R² = 0.53501
KOMP Lines
y = 0.8281x + 0.1882
R² = 0.55329
Femur TV Ratio, (test/control)
Body Weight Ratio, (test/control)

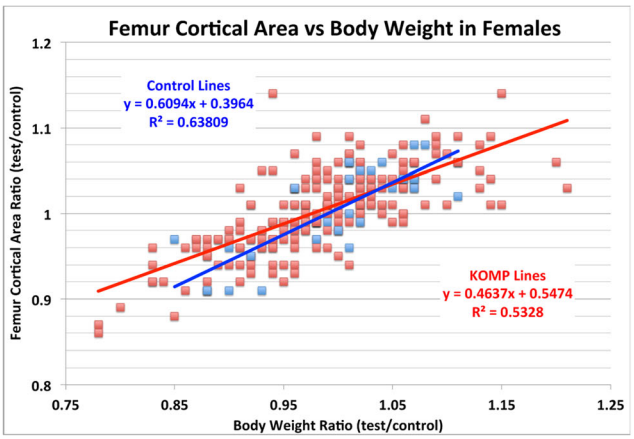
Femur Cortical Area vs Body Weight in Females
Control Lines
y = 0.6094x + 0.3964
R² = 0.63809
KOMP Lines
y = 0.4637x + 0.5474
R² = 0.5328
Femur Cortical Area Ratio (test/control)
Body Weight Ratio (test/control)

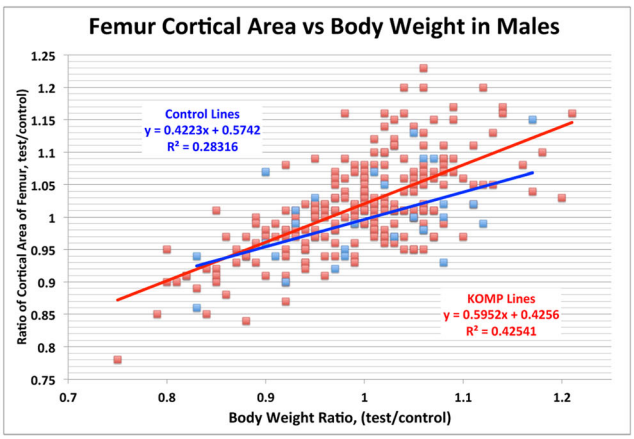
Femur Cortical Area vs Body Weight in Males
Control Lines
y = 0.4223x + 0.5742
R² = 0.28316
KOMP Lines
y = 0.5952x + 0.4256
R² = 0.42541
Ratio of Cortical Area of Femur, test/control)
Body Weight Ratio, (test/control)

◀ **Fig. 1** **a** Relationship between trabecular BV/TV of the femur and L4 vertebra versus body weight. The ratio of the mean test sample BV/TV to the mean value of the BV/TV from C57BL/6NJ control group is plotted on the vertical axis against the ratio of the test sample body weight divided by the mean value of the body weight from C57BL/6NJ control group (horizontal axis). KOMP lines are plotted in red and the control lines are in blue. **b** Relationship between total volume (TV) of the trabecular compartment ROI and subperiosteal area, Tt.Ar (abbreviated as total area, TA) of the femur versus body weight. The ratio of the mean test sample TV and TA to the mean value of the TV and TA from C57BL/6NJ control group (vertical axis) is plotted against the ratio of the test sample body weight divided by the mean value of the body weight from C57BL/6NJ control group (horizontal axis). KOMP lines are plotted in red and the control lines are in blue

Because of the dimorphisms, the list of top 10 KOMP genes for low and high BV/TV differs between male and female lines (Fig. 3). The arrows point to KOMP lines that are previously documented in the literature such as *Irf8* [28], *Osm* [29], and *Spp1* [30]. The list emphasizes the large percentage of unknown or unappreciated genetic loci that can impact skeletal variation. To examine a specific gene, double click the gene abbreviation and the BV/TV value of the KOMP line is plotted within the frequency distribution of the control and all the KOMP lines. From the tab at the top of the page, all the summary data and detailed graphical data can be followed (Fig. 2b). The summary table tab provides links to view the primary data that lead to the call of a measure being normal, high, or low, and a video is available to demonstrate how this feature is navigated. The links tab presents both IMPC and web links that provide context to the gene and its potential relevance to understanding the skeletal phenotype. A video is present to demonstrate how the page is intended to provide background information. The page reveals that most of the BV/TV variation as determined by μCT was not identified by the DXA particularly when the direct measurement of bone mineral content was employed. Many of the genes were identified in GWAS studies but only a few were associated with a bone phenotype. One exception was the *Rin3* gene, which will be discussed later. OMIN is another source that can identify human disorders that have been linked to a specific gene. However, none on the list that had an OMIN entry described a bone abnormality. The literature search can also provide potential mechanisms or pathways that might explain the phenotype. For example, the *Cp* gene leads to the development of hemochromatosis in which the high intracellular ferritin can be inhibitory to osteogenesis [31] and may account for the association with a low BV/TV phenotype. In contrast, the *Elk1* gene, which is androgen regulated and essential for CSF1-dependent osteoclastogenesis [32], is associated with male-restricted high bone mass. However, other KOMP lines examined were inconsistent with published literature. For example, *Adora* is described to have a low bone mass [33] but in our analysis, it did not meet statistical significance. The *Gpnmb* (osteoactivin) knockout has been extensively studied in a naturally occurring mutation that arose in a DBA background [34]. Although the KOMP-derived mouse has a trend in the same direction, the phenotype is limited to the female femur raising the possibility that other background genes could be responsible for the disparity between the published and KOMP-derived line.

Table 1 Impact of body weight on bone μCT architectural measurements

Measurement	Group	Sex	Y	R^2
Femur BV/TV	Control	Female	0.89× + 0.14	0.17
	Control	Male	0.91× + 0.09	0.22
	KOMP	Female	0.34× + 0.77	0.02
	KOMP	Male	1.14× - 0.05	0.19
Vertebral BV/TV	Control	Female	0.71× + 0.30	0.28
	Control	Male	0.31× + 0.68	0.08
	KOMP	Female	0.37× + 0.63	0.07
	KOMP	Male	0.47× + 0.54	0.11
Femur cortical area	Control	Female	0.61× + 0.40	0.64
	Control	Male	0.42× + 0.57	0.28
	KOMP	Female	0.46× + 0.55	0.53
	KOMP	Male	0.60× + 0.43	0.42
Femur total volume	Control	Female	0.80× + 0.21	0.68
	Control	Male	0.69× + 0.30	0.54
	KOMP	Female	0.72× + 0.29	0.58
	KOMP	Male	0.83× + 0.19	0.55

This gene-by-gene examination can be extended to the other measures of bone size or body size but only adds to the overwhelming complexity and disorganization in utilizing a screening platform in an effective manner. It becomes a matter of chance that a gene of interest will be identified that is worthy of a more detailed analysis. We wanted to explore whether there are patterns of bone architecture, bone, and body size associated with histomorphometric findings that are recognizable and provide a mechanistic strategy to bring a degree of order into the screening process.

Classifications Based on Micro-Computed Tomography and Body Size Measurements

The search page of the web portal allows for a logical "AND" search for the three major categories and an "OR" search within a specific category of the data obtained by the screening protocol. From this double search, two major subcategories are defined as low or high bone mass encompassing KOMP lines that demonstrate either a significant variation of BV/TV and/or femur size. In the case of low bone mass (LBM), there are nine lines with a low BV/TV but otherwise have normal or high values of bone and body size (Fig. 4a).

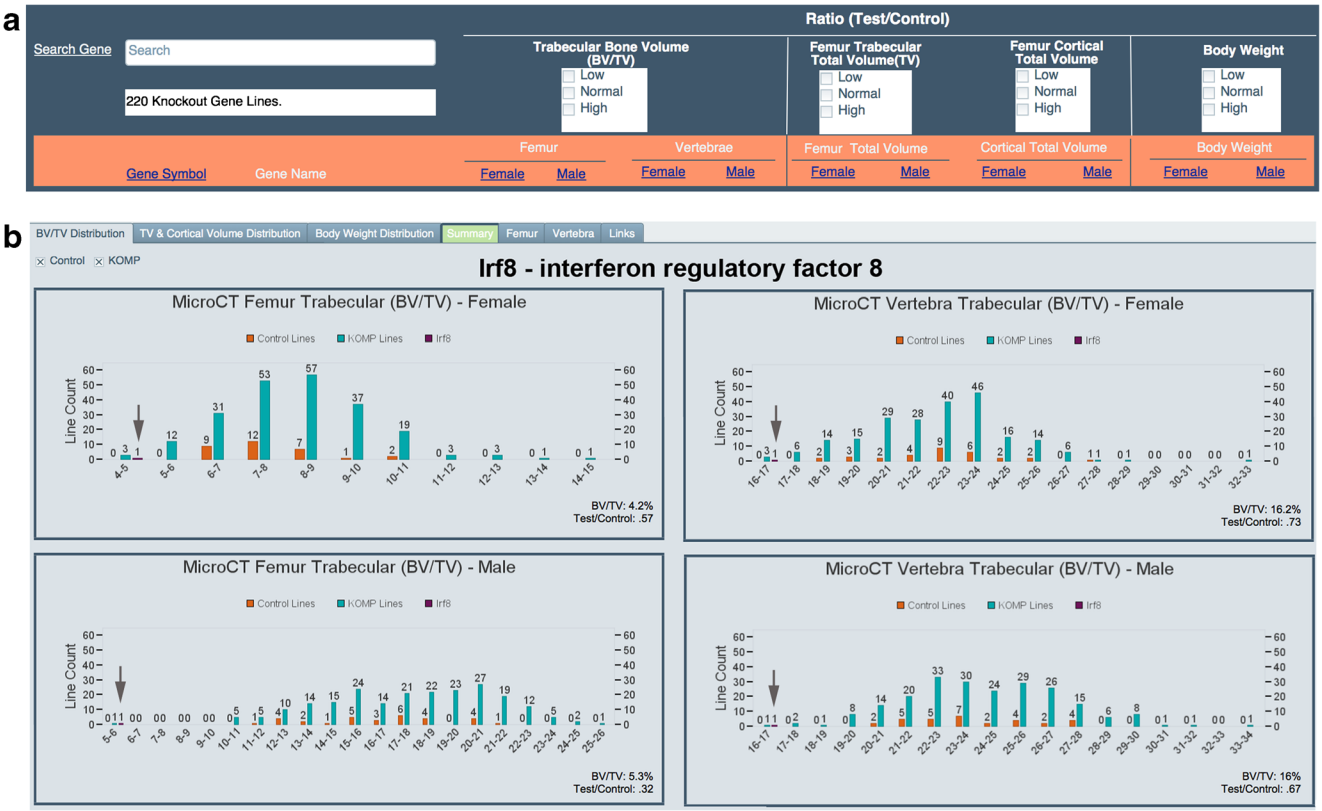

Fig. 2 **a** Search page interface. By checking the various boxes, the KOMP lines that were called low, normal, or high for each measurement category (BV/TV, femur TV and cortical area, body weight) will be returned. The ratios of the test vs control value that are called as being a meaningful variant are highlighted. The relative rank of each category can be observed by sorting the list, which is performed by clicking the hyperlinked female and male header for each category. Individual genes can be examined by entering the gene symbol in the search gene field. When any one box is checked within one category, no restraint is placed on the other search criteria. When one box is checked in more that one category, an "AND" search is performed. When two criteria are clicked within a single category, then an "OR" search is performed. **b** Frequency distribution graphic of the BV/TV measurement of the *Irf8* KOMP line as found in the femur and vertebra of female and male mice. The plot of the test value (magenta bar beneath the arrow) can be compared to controls only (brown), all KOMP lines (green), or both. In the lower right of each graphic is the measured BV/TV value and the calculated test/control value of the KOMP line. The same graphic can be viewed for the femur TV and TA and the body weight by selecting the tabs at the top of the page

The low values that exceed normal variation are highlighted in yellow and again show dimorphism in sex and site. The ability to include the normal or high criteria identifies *Irf8* as having a high cortical total volume (magenta), which as discussed later, is a reflection of the cortical bone remodeling in response to the high osteoclastic activity in this KOMP line. It also draws

Table 2 Sex and site dimorphism of bone volume, bone size, and body weight

	Total number		Female only	Male only	Both sexes
Low BV/TV	19	Femur only	4–0	10	0
		Vertebra only	3–4	2	1
		Both sites	3	1	1
High BV/TV	29	Femur only	20	8	4
		Vertebra only	1	5	0
		Both sites	0	4	0
Low FTV	4	Femur only	2	0	2
High FTV	5	femur only	0	5	0
Low CV	5	Femur only	0	4	1
High CV	19	Femur only	1	17	1
Low BW	24	Weight only	6	12	6
High BW	16	Weight only	7	6	3

A. Low Female BV/TV

	Gene Symbol	Gene Name	Femur Female	Vertebrae Female
1	Irf8 ←	interferon regulatory factor 8	0.57	0.73
2	Htr1d	5-hydroxytryptamine (serotonin) receptor 1D	0.66	0.79
3	Moxd1	monooxygenase, DBH-like 1	0.68	0.85
4	Dnajc5g	DnaJ (Hsp40) homolog, subfamily C, member 5 gamma	0.73	0.91
5	Gpnmb ←	glycoprotein (transmembrane) nmb	0.74	0.96
6	Cited4	Cbp/p300-interacting transactivator, with Glu/Asp-rich carboxy-terminal	0.74	0.86
7	Rab36	RAB36, member RAS oncogene family	0.74	0.77
8	Arrb1	arrestin, beta 1	0.77	0.73
9	Rab3c	RAB3C, member RAS oncogene family	0.97	0.77
10	Vcpkmt	Vcpkmt<tm1.1(KOMP)Vlcg>/J	0.86	0.80

B. Low Male BV/TV

	Gene Symbol	Gene Name	Femur Male	Vertebrae Male
1	Irf8 ←	interferon regulatory factor 8	0.32	0.67
2	Dnajb3	DnaJ (Hsp40) homolog, subfamily B, member 3	0.62	0.81
3	Tmem136	transmembrane protein 136	0.62	0.80
4	Hspb3	heat shock protein 3	0.62	0.96
5	Ceacam16	CEA-related cell adhesion molecule 16	0.62	0.81
6	Cp	ceruloplasmin	0.63	0.74
7	Arrb1	arrestin, beta 1	0.69	0.78
8	Ghsr	growth hormone secretagogue receptor	0.70	0.90
9	Tprn	taperin	0.78	0.79
10	Eif1b	eukaryotic translation initiation factor 1B	0.95	0.75

C. High Female BV/TV

	Gene Symbol	Gene Name	Femur Female	Vertebrae Female
1	Rin3	Ras and Rab interactor 3	1.95	1.04
2	R3hcc1l	R3hcc1l<tm1b(KOMP)Wtsi>/J	1.78	1.01
3	Fam186b	family with sequence similarity 186, member B	1.69	1.07
4	Osm ←	oncostatin M	1.66	1.19
5	Lipn	lipase, family member N	1.62	1.18
6	Ocstamp	Ocstamp, osteoclast stimulatory transmembrane protein	1.50	1.18
7	Try4	trypsin 4	1.50	1.00
8	Spp1 ←	secreted phosphoprotein 1	1.50	1.02
9	Tex29	testis expressed 29	1.45	1.14
10	Slc8a3	solute carrier family 8 (sodium/calcium exchanger),	1.41	1.45

D. High Male BV/TV

	Gene Symbol	Gene Name	Femur Male	Vertebrae Male
1	Elk1	ELK1, member of ETS oncogene family	1.58	1.23
2	Akap11	A kinase (PRKA) anchor protein 11	1.51	1.22
3	Ptpru	protein tyrosine phosphatase, receptor type, U	1.49	1.14
4	R3hcc1l	R3hcc1l<tm1b(KOMP)Wtsi>/J	1.46	1.12
5	Rin3	Ras and Rab interactor 3	1.43	1.05
6	Mfsd10	major facilitator superfamily domain containing 10	1.42	1.19
7	Tex29	testis expressed 29	1.41	1.17
8	Slc46a3	solute carrier family 46, member 3	1.40	1.23
9	Mettl21c	methyltransferase like 21C	1.38	1.13
10	C1qb	complement component 1, q subcomponent, beta polypeptide	1.37	1.22

Fig. 3 Top 10 hits for BV/TV in male and female KOMP lines. This is a composite of screen shots from the search page to illustrate the lines with the greatest variation of the femur and vertebra BV/TV value. The arrows point to previously published mutant mouse lines. The low/high call ratio for female femur is 0.75/1.45 femur and 0.80/1.20 for female vertebra, while the low/high ratio for male femur is 0.70/1.35 and 0.80/1.20 for male vertebra

attention to *Dnajc5g* with the high body weight in females that may be responsible for a similar finding in humans [35]. The second subgroup of LBM is the six KOMP lines with low BV/TV and either low bone size, low body size, or both (Fig. 4b). In some cases, a potential explanation for the association exists such as the *Ghsr* (ghrein receptor), which can be a cause of partial growth hormone deficiency [36], but in most cases, the mechanism is not obvious. The third subgroup of LBM includes KOMP lines with a normal BV/TV but low bone or body size (Fig. 4c). Note that two of these lines, *Pitx3* and *Akr1b8*, have a BV/TV that is relatively high, further contradicting the association of low BV/TV with a small bone or somatic size. *Pitx3* is a well-studied knockout line known primarily for its role in midline neurological structures, which potentially could contribute to impaired pituitary function. The gene also has an important role for skeletal muscle differentiation, which could contribute to the small body and bone size but does not appear to impact the trabecular bone compartment. There is no obvious explanation for the *Akr1b8* phenotype.

Similarly, the high bone mass group (HBM) can be subgrouped into those with high BV/TV only. Figure 5a lists 10 of 18 KO lines with isolated high BV/TV, 7 of which are in the top 10 list including the 2 previously known genes (*Osm* [29] and *Spp1* [30]). There are nine genes that have a high BV/TV and large bone size with either normal or high body weight (Fig. 5b). The third category of HBM with normal BV/TV but high bone and or body size has seven lines. Only one within the HBM group was detected by the DXA study (*Bzw2*) by its bone mineral content or increased lean body mass.

Finally, it should be noted that a number of KOMP lines demonstrated significant variation in body weight (high and low) without an impact on the bone architectural measurements although a few show a trend in the same direction but were not deemed significant (see supplemental data, Fig. 2).

a

LBM: LBV/TV, NTV, NTA, NWt

Gene Symbol	Gene Name	Femur BV/TV Female	Femur BV/TV Male	Vertebrae BV/TV Female	Vertebrae BV/TV Male	Femur Total Volume Female	Femur Total Volume Male	Cortical Total Volume Female	Cortical Total Volume Male	Body Weight Female	Body Weight Male
Irf8	interferon regulatory factor 8	.57	.32	.73	.67	1.12	1.09	1.14	1.08	.94	.92
Ceacam16	CEA-related cell adhesion molecule 16	1.03	.62	1	.81	.98	.89	1.01	.93	.92	.87
Dnaib3	DnaJ (Hsp40) homolog, subfamily B, member 3	.81	.62	.9	.81	1.06	.98	1.06	.97	1.2	1.02
Tmem136	transmembrane protein 136	.84	.62	.87	.8	.93	.94	.96	.96	.98	1.03
Cp	ceruloplasmin	.86	.63	.86	.74	1	.95	.98	.91	.99	.96
Moxd1	monooxygenase, DBH-like 1	.68	.8	.85	.87	.9	.96	.97	1	.87	.93
Dnajc5g	DnaJ (Hsp40) homolog, subfamily C, member 5 gamma	.73	.86	.91	.97	1.02	1.05	1.03	1.01	1.04	1.03
Cited4	Cbp/p300-interacting transactivator, with Glu/Asp-rich carboxy-terminal	.74	.96	.86	.96	.97	.96	.99	.97	.98	1.03
Gpnmb	glycoprotein (transmembrane) nmb	.74	.95	.96	.94	.9	.95	.92	.95	.95	1.04

b

LBM: LBV/TV, LTV, LTA, LWt

Gene Symbol	Gene Name	Femur BV/TV Female	Femur BV/TV Male	Vertebrae BV/TV Female	Vertebrae BV/TV Male	Femur Total Volume Female	Femur Total Volume Male	Cortical Total Volume Female	Cortical Total Volume Male	Body Weight Female	Body Weight Male
Hspb3	heat shock protein 3	.89	.62	.94	.96	.95	.89	.97	.91	.88	.82
Htr1d	5-hydroxytryptamine (serotonin) receptor 1D	.66	.75	.79	.93	.85	.84	.88	.9	.85	.8
Rab36	RAB36, member RAS oncogene family	.74	.79	.77	.91	.92	.86	.94	.91	.92	.85
Arrb1	arrestin, beta 1	.77	.69	.73	.78	.84	.8	.87	.85	.78	.79
Ghsr	growth hormone secretagogue receptor	1.11	0.70	1.15	0.90	.94	.87	.98	.89	1	.83
Vcpkmt	Vcpkmt<tm1.1(KOMP)Vlcg>/J	0.86	0.83	0.80	0.83	.94	.88	.91	.84	.86	.88

c

LBM: NBV/TV, LTV, LTA, LWt

Gene Symbol	Gene Name	Femur BV/TV Female	Femur BV/TV Male	Vertebrae BV/TV Female	Vertebrae BV/TV Male	Femur Total Volume Female	Femur Total Volume Male	Cortical Total Volume Female	Cortical Total Volume Male	Body Weight Female	Body Weight Male
Akr1b8	aldo-keto reductase family 1, member B8	1.35	.93	.96	.96	.82	.8	.89	.87	.8	.92
Slc1a1	solute carrier family 1 (neuronal/epithelial high affinity	1.09	.92	.99	.92	.8	.83	.91	.9	.88	.85
Adck2	aarF domain containing kinase 2	.86	1.02	.84	1.09	.84	.79	.92	.9	.84	.81
Acsf2	acyl-CoA synthetase family member 2	1.18	.94	1.19	.99	.9	.81	.95	.85	.92	.84
Pitx3	paired-like homeodomain transcription factor 3	1.28	.8	1	.96	.86	.77	.86	.78	.78	.75

Fig. 4 **a** Screened KOMP lines fulfilling the category of low mass (LBM) in the subcategory of low BV/TV (LBV/TV) with either normal or high values in the other measurements (NTV normal total volume of the diaphyseal ROI, NTA normal subperiosteal area, Tt.Ar, NWt normal weight). The low values are highlighted with yellow, while the high value outliers are highlighted in magenta. **b** Screened KOMP lines fulfilling the category of low mass (LBM) in the subcategory of low BV/TV and low values in one or more of the other measurements. **c** Screened KOMP lines fulfilling the category of low mass (LBM) in the subcategory of a normal BV/TV and low values in one or more of the other measurements. The two KOMP lines with a relatively high BV/TV are circled

Addition of Histomorphometry to the Architectural/Somatic Classification

Static, dynamic, and cellular histomorphometry was performed on many of the KOMP lines that had significant variation in the bone architectural measurements. The web portal provides the primary data for these measurements (summary table) and collates them in a horizontal slider graph format that also includes the μCT and body weight measurements (Fig. 6). The histological method does not produce the traditional visual measures of osteoblast or osteoclast surfaces, or erosion surfaces. Instead, AP activity is used to identify all cells in the osteoblast lineage. Bone surfaces actively making bone matrix meet the criteria of an AP+ surface overlying a mineralization line, while bone lining cells are identified as AP+ but over a non-mineralizing surface. Similarly, cells in the osteoclast lineage are identified by their TRAP activity. They are partitioned into bone resorbing cells (TRAP+ over a

a **HBM:HBV/TV, NTV, NTA, NWt**

Gene Symbol	Gene Name	Femur BV/TV		Vertebrae BV/TV		Femur Total Volume		Cortical Total Volume		Body Weight	
		Female	Male	Female	Male	Female	Male	Female	Male	Female	Male
Rin3	Ras and Rab interactor 3	1.95	1.43	1.04	1.05	1.02	1.08	1.03	1.07	.98	1.09
R3hcc1l	R3hcc1l<tm1b(KOMP)Wtsi>/J	1.78	1.46	1.01	1.12	1.04	.99	1.02	1.02	1.03	1
Osm	oncostatin M	1.66	1.2	1.19	1.38	1.01	.9	1.03	.95	.96	.8
Lipn	lipase, family member N	1.62	1.29	1.18	1.12	1.05	1.07	1.09	1.11	1.01	1.06
Akap11	A kinase (PRKA) anchor protein 11	1.26	1.51	.82	1.22	.92	.99	.94	1.03	.94	.97
Ocstamp	Ocstamp, osteoclast stimulatory transmembrane protein	1.5	.86	1.18	.87	1.04	.98	1.05	.99	.98	.91
Spp1	secreted phosphoprotein 1	1.5	1.32	1.02	1.13	1.01	1.07	.97	1.01	.98	1.06
Try4	trypsin 4	1.5	1.28	1	1.08	1.03	1.03	1.01	1.02	1.02	1.01
Mfsd10	major facilitator superfamily domain containing 10	1.28	1.42	1.18	1.19	1	1.12	1.01	1.11	1.02	1.08
Slc46a3	solute carrier family 46, member 3	1.18	1.4	1.15	1.23	1.08	1.09	1.08	1.09	1.02	1.09

b **HBM:HBV/TV, HTV, HTA, HWt**

Gene Symbol	Gene Name	Femur BV/TV		Vertebrae BV/TV		Femur Total Volume		Cortical Total Volume		Body Weight	
		Female	Male	Female	Male	Female	Male	Female	Male	Female	Male
Fam186b	family with sequence similarity 186, member B	1.69	1.23	1.07	1.02	1.09	1.18	1.09	1.17	1.11	1.14
Elk1	ELK1, member of ETS oncogene family	.99	1.58	1.08	1.23	.93	1.22	.98	1.2	.97	1.04
Ptpru	protein tyrosine phosphatase, receptor type, U	1.14	1.49	1.08	1.14	1.02	1.15	1.01	1.16	1.14	.98
Tex29	testis expressed 29	1.45	1.41	1.14	1.17	1.02	1.18	1.01	1.15	1.03	1.07
Mettl21c	methyltransferase like 21C	1.15	1.38	1.01	1.13	1.05	1.19	1.06	1.17	1.07	1.09
Plekha3	pleckstrin homology domain-containing, family A	1.01	1.36	.99	1.18	1.07	1.25	1.08	1.23	1.06	1.06
Bex4	brain expressed gene 4	1.32	1.37	1.06	1.13	1.08	1.22	1.06	1.16	1.11	1.21
Slc8a3	solute carrier family 8 (sodium/calcium exchanger),	1.41	1.30	1.45	1.22	1.05	1.19	1.07	1.16	.96	1.04
Ccdc120	coiled-coil domain containing 120	1.23	1.34	1.20	1.21	1.12	1.16	1.08	1.16	1.13	1.14

c **HBM:NBV/TV, HTV, HTA, NWt**

Gene Symbol	Gene Name	Femur BV/TV		Vertebrae BV/TV		Femur Total Volume		Cortical Total Volume		Body Weight	
		Female	Male	Female	Male	Female	Male	Female	Male	Female	Male
Arsk	arylsulfatase K	.91	.96	1.04	1.03	1.16	1.04	1.11	1.02	1.08	1.03
Rps6kl1	ribosomal protein S6 kinase-like 1	1.16	1.05	1.11	1	1.15	1.08	1.07	1	1.1	1.05
Zfp40	zinc finger protein 40	1.09	1.33	.91	1.13	1.09	1.24	1.07	1.2	1.01	1.12
Hsd17b11	hydroxysteroid (17-beta) dehydrogenase 11	1.41	1.26	1.05	1.1	.87	1.13	.97	1.16	.94	1.02
Zfp961	Zfp961<tm1.1(KOMP)Mbp>/J	1.14	1.22	.92	1.04	.97	1.16	.97	1.15	.93	1.03
Lrch1	leucine-rich repeats and calponin homology (CH) domain containing 1	1.03	1.13	1	.98	1.11	1.13	1.09	1.15	1.09	1.09
Bzw2	basic leucine zipper and W2 domains 2	1.32	1.27	.97	1.08	1.13	1.27	1.14	1.2	1.15	1.06

Fig. 5 **a** Screened KOMP lines fulfilling the category of high bone mass (HBM) in the subcategory of high BV/TV and either normal or low values in the other measurements (NTV normal total volume of the diaphyseal ROI, NTA normal subperiosteal area, Tt.Ar, NWt normal weight). The high value outliers are highlighted in magenta, while the low value outlier is highlighted in yellow. **b** Screened KOMP lines fulfilling the category of HBM in the subcategory of high BV/TV and high values in one or more of the other measurements. The circled value for vertebral BV/TV in *Ccdc120* is an example of a result that met the ratio requirement of being ≥ 1.20 but failed the statistical test of being ≤ 0.0001. **c** Screened KOMP lines fulfilling the category of normal bone mass (NBM) in the subcategory of normal BV/TV and high values in one or more of the other measurements

non-mineralizing surface) and bone remodeling cells (TRAP+ over a mineralizing surface). Finally, focal regions where AP, TRAP, and a mineralization line co-localize are considered as a surrogate for a bone remodeling unit.

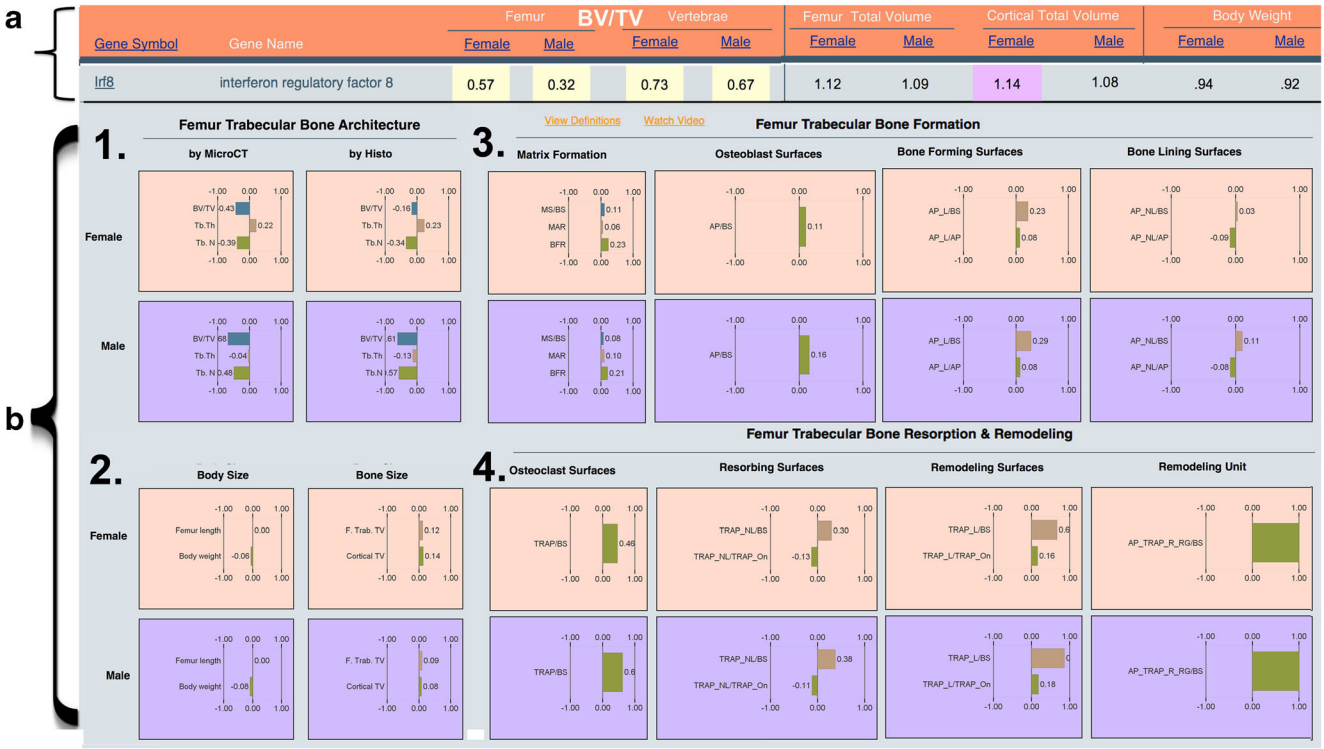

Fig. 6 Summary graphic of all the architectural and histomorphometric measurements of the *Irf8* KOMP line. The top panel (**a**) presents the ratio values obtained from the search page and the horizontal bar graphic below (**b**) is reached by entering the detail pages and clicking the femur tab. The same graphic can be seen for the vertebral measurements by clicking the vertebra tab. Male and female values are color-coded and there are four sections with four or eight boxes per section. The bars project to the right or left by the fraction that they extend above or below the mean value of the control measurement. Thus, the highlighted BV/TV ratio of 0.32 for the male femur in search page is shown as − 0.68 in the horizontal bar graph of the upper left section (1. bone architecture), while the female femur total volume and total cortical areas of 1.12 and 1.14 of the search page project to the right as 0.12 and 0.14 of the lower left section (2. bone and body size). The two sections on the right present histomorphometric information. The upper section (3) shows the dynamic measurement based on the fluorescent mineralization lines (matrix formation) and total osteoblast lineage surfaces (AP positive surfaces). The distribution of the AP-positive surfaces to a labeling or mineralization-inactive surface is used to discriminate bone-forming or bone-lining surfaces. The brown bar is the fraction of the total surfaces that are AP positive while the green bar is the fraction of the total AP signal that is on a forming or lining surface. Thus, in the example presented, there is a greater proportion of the AP-positive surfaces on the labeling versus the lining surfaces. The lower section (4) presents the osteoclast-derived information. The total osteoclast surface is the fraction of all bone surfaces associated with the TRAP signal. This signal is divided into TRAP-positive surface that is associated with a mineralization line (bone remodeling) or without a mineralization line (bone resorbing) in the brown bar and the fraction of the total TRAP signal that is assigned to either compartment (green bar). Thus, in this KOMP line, a greater proportion of the greatly expanded total TRAP signal is associated with a mineralizing (remodeling) surface. The far right graphic represents the remodeling unit measurement as identified by focal areas where the AP, TRAP, and mineralization signals coincide. It is expressed as the fraction of the surface that has these three signals in the KOMP line versus the same measurement of the control lines, and in this case, the value is extremely high

The application of this histological approach is illustrated for the *Irf8* line since it has been well characterized to have a low trabecular bone mass secondary to an activated osteoclast lineage resulting from the loss of the negative regulatory action of Irf8 on the expression of nuclear factor of activated T cells c1 (*NFATc1*, [37]). The KOMP line also demonstrates a very low BV/TV in all bone compartments and in both sexes. Figure 6 summarizes the architectural features by μCT and histomorphometry of the female and male femur, and the same graphic is also presented for the vertebral compartment on the web portal. On the left upper four-box compartment, the bone architectural measurements by μCT and histomorphometry show the bar extending to the negative side of the normal value for trabecular number and BV/TV. In both cases, the bone volume, cortical area, and somatic sizes do not vary significantly (lower four boxes). The dynamic and cellular measurements are shown in the 16 boxes to the right side of the figure with osteogenic measures in the upper panel and the osteoclast and remodeling units in the lower panels. The striking feature is the high number of osteoclast surfaces that are more prominent on remodeling surfaces than resorbing surfaces. The net bone formation, as assessed by dynamic labeling to yield the BFR, is modestly increased while the osteoblasts are more prominent on bone forming than inactive bone-forming surfaces. Most striking is the very high bone remodeling unit measurement indicating a high turnover state. The pathophysiological mechanism of the *Irf8* is high osteoclastogenesis adjacent to Rankl-expressing cells [37], which would be within the environment of a bone remodeling unit.

Table 3 Histological subgroup within the LBM group

Process	Osteoblast activity	Osteoclast activity	KOMP lines
(1) High remodeling (high turnover)	• Normal to high BFR • High activated osteoblasts • High remodeling units	• Normal to high osteoclast surfaces • High remodeling units	*Irf8*, *Htr1d*
(2) Low modeling (adynamic bone)	• Low to normal BFR • Low to normal activated osteoblasts • Low remodeling units	• Low to normal osteoclast surfaces • Low remodeling units	*Ceacam16*, *C19Rik*, *Arrb1*, *Rab36*, *Tpm*, *Ahrr*, *Vcpkmt*
(3) Low modeling (uncoupling)	• Low to normal BFR • Low to normal activated osteoblasts • High remodeling units	• Normal to high osteoclast surfaces • High remodeling units	*Dnajb3*, *Hspb3 (femur)*, *Tmem136*, *Pitx3*
(4) Impaired osteoblast function	• Normal to low BFR • Normal to high activated osteoblasts • High remodeling units	• Normal to low osteoclasts surfaces • High remodeling units	*Cp*

The dynamic and cellular measurements were used to subcategorize the LBM group based on the rationale that the low bone volume would be expected to elicit a strong osteoblastic response (Table 3). The reasons why the low bone mass persists can be divided into four subgroups (Tables 3). First, the osteoclastic activity does induce an osteoblast response but it is insufficient to correct the defect. This results in a high bone turnover phenotype with high bone formation, activated osteoblast in association with high osteoclast, and high remodeling units. Besides the *Irf8* KOMP line described above, the *Htr1d* also falls in this category.

The second histological grouping that is associated with the LBM classification is an adynamic state characterized by a minimal change in the bone forming and active osteoblast markers and low osteoclastic activity. The key feature is a very low bone remodeling unit value. This was the most common classification in the LBM group examined to date.

The third histological presentation in the LBM category is interpreted as impaired osteoblast coupling from activated osteoclast. Bone formation is low and the osteoblast lineage is inactive even though osteoclasts are present and remodeling units are moderately elevated. Because this is not a high bone turnover state, the moderate increase in osteoclast resorbing activity is not compensated by an osteoblast response. This was the second most common classification.

The fourth category differs from the others in that bone formation is low but the osteoblast lineage is activated with high remodeling units but with low osteoclastic activity. This pattern may reflect a defect in bone matrix production where active osteoblasts are present and osteoclasts are low, yet net bone formation is not present. The only line that fell into this group was *Cp*, which indirectly leads to hemochromatosis in which the high intracellular ferritin can compromise osteoblast function [31].

The rational for segmenting the HBM group is based on expectation that the osteoclast lineage should be activated in an attempt to prevent excessive bone matrix accumulation and to remodel the bone to maintain mechanical integrity [38]. Three categories based on the magnitude of bone remodeling and modeling were identified to be associated with a HBM phenotype (Table 4). The first and most populated group is characterized by low remodeling due to a low osteoclast number. Bone formation and osteoblast activation and bone remodeling units are all low despite the high total bone volume. The second grouping is another mechanism for low bone remodeling. Although the

Table 4 Histological subgroup within the HBM group

Process	Osteoblast activity	Osteoclast activity	KOMP lines
(1) Low remodeling–low Oc surfaces	• Normal to low BFR • Low active osteoblasts • Normal to low remodeling units	• Normal to low osteoclast surfaces • Normal to low remodeling units	*R3hcc1*, *Fam186b*, *Osm*, *Lipn*, *Elk1*, *Akap11*, *Try4*, *Tex29*, *Neurl2*, *Mfsd10*, *Ces4a*, *Pycr1*, *Sptssb*, *Il24*, *Bzw2*
(2) Ineffective remodeling–normal Oc surfaces	• Normal to low BFR • Low active osteoblasts • High remodeling units	• Normal to high osteoclast surfaces • High remodeling units	*Ocstamp*, *Ptpru*, **Hsd17b11*, *Ccdc120*, *Tspan*, **Dixdc1*
(3) Continued modeling	• Normal to high BFR • High active osteoblasts • Low remodeling units	• Low osteoclast surfaces • Low remodeling	*Rin3*

measures of bone formation and activated osteoblasts are low, the osteoclast number and remodeling units are high. We interpret this combination as ineffective remodeling that might occur by functional defect of the osteoclast to degrade bone matrix. Within this group is *Ocstamp*, which has been shown to have impaired bone resorbing properties due to a defect in osteoclast fusion [39].

The third group, which was defined by *Rin3*, is particularly interesting because it appears to be an example of continuing bone modeling. Unlike the other cases in which the measures of bone matrix formation are low, *Rin3* has high bone formation, activated osteoblast, and high remodeling in the context of low osteoclast surfaces. This is a pattern that is expected during somatic growth when bone modeling builds bone mass but would be expected to be downregulated once maturity is reached. However, the underlying mechanism in this case may be derived from the osteoclast lineage, such as coupling, since the literature has identified point mutations within the gene that are associated with Paget's disease [40] as well as GWAS hits that link the gene to Paget's disease and high bone mass [41, 42].

Discussion

The experience of the IMPC, other bone screening projects, clinical genetic units, the GWAS group, and numerous investigator-initiated studies indicate that there will be an overwhelming number of genes that can impact bone mass variation. This emerging reality probably explains the high polymorphic basis for bone disease in humans and confounds efforts based on exome and whole-genome sequencing to be predictive of personalized risk for developing bone disease. Progress towards the ultimate goal of providing a personalized risk assessment and therapeutic modality will require knowing the impact and molecular mechanism of each genetic element on bone variation. This is a big data problem and will require applying the principles of big data management and organization. The IMPC is providing the fundamental experimental platform, and the bone community needs to develop an effective mechanism to screen, present, and interpret the KO lines that have an impactful effect on factors affecting skeletal health.

Design of the Screening Program

Given the number of IMPC lines that will have to be screened, a balance between throughput and sensitivity of the screening has to be reached. Although the whole-body DXA performed by the IMPC is reporting over 300 lines on their portal (http://www.mousephenotype.org/data/phenotypes/MP:0010122), our analysis using μCT indicates that most of the cases in which the trabecular component of the bone is abnormal are not being detected by DXA. Those that are identified appear to have variation in bone size or the animal having low or high body weight [43•]. Furthermore, μCT reveals that variation in the trabecular and cortical measurements exceed the variance usually observed in published studies particularly in male animals. In addition, the architectural measurements are strikingly dimorphic for the sex and bone compartment. The latter is not unexpected since the axial and appendicular lineages have different embryological origins and thus different genetic mechanism for skeletal homeostasis. Thus, to capture the full spectrum of the skeletal architecture, the screen should include a minimum of eight animals from each sex and both axial and appendicular bone should be examined.

Besides identifying KOMP lines with significant variation, the screen may have resolved one of the questions regarding the relationship between body size and bone measurements. The lack of a significant correlation between BV/TV in either compartment to body weight is a significant observation. Mice with small body size did not have a corresponding low BV/TV measurement. However, there was a modest relationship between femur bone size and both total area selected within the ROI of the distal femur and the mid cortical bone area with body weight. Whether there should be a correction factor to these measures based on weight for selecting a line as being variant is debatable since a number of KOMP lines showed significant body weight variation without a change in BV/TV or bone size (supplemental data, Fig. 2).

There are limitations to the screen that still need to be addressed. The most glaring one is the impact of different microbiomes at the different analysis locations have on skeletal measurements [44–46]. The use of the same control lines within the 11-phenotyping centers is the best solution to date, but site variation of control values between sites is well documented on the IMPC site. (http://www.mousephenotype.org/data/phenotypes/MP:0010122). Bone architecture and presumably dynamic/cellular histomorphometry will be particularly sensitive to differences in microbiome composition. Another variable is the molecular mechanism of the gene inactivation, which is a concern of IMPC such that many of the IMPC lines are being regenerated using CRISPR/Cas9. Thus, a repeat of the current KOMP lines using the new standard for gene inactivation may be required.

A strong case can be made that the screen should be based on the mechanical/material properties of bone [16•]. This is an approach being used at the IMPC bone group at Wellcome Trust Sanger Institute (http://www.boneandcartilage.com/currentwork.html). When used in conjunction with μCT, it is useful to detect abnormalities of cortical bone that may not be appreciated by the architectural measurements [47]. Another approach might include an assessment of bone mineral composition. However, neither of these methods are high throughput. Others have argued that selecting mice at 12 weeks of age when they are at peak bone mass is not optimal for gene discovery because aging the mice will reveal abnormalities that would not be apparent at the earlier

time in life. This is a cost question of maintaining a minimum of four cages (four mice per cage) per time point for 2 months (12 weeks of age) versus 5 months (6 months of age) or even longer. For both the suggestion of mechanical properties or changes with aging, we believe the most cost-effective approach is to focus on IMPC lines that show a significant variant at the time of peak bone accumulation to identify IMPC lines likely to have an abnormality in material/mechanical properties or predisposition for susceptibility or resistance to bone disease with advancing age.

The one additional test that was performed in mice with a significant variation was histomorphometry of the trabecular bone. The fundamental features of this methodology are the relative speed and throughput of the sectioning/imaging procedures relative to traditional plastic/paraffin-embedded tissue and the observer-independent computer analysis of the resulting computer-controlled imaging acquisition. The ability to make corrections to the staining and imaging protocol as well as alteration in the computer algorithms was based on the application of the analysis to the monthly controls. For example, control measures of image intensity of the test samples and reference standard were incorporated to detect technical issues affecting the image acquisition. As changes to analysis algorithms were developed, the entire control and KOMP dataset was recalculated to remain consistent in the analysis through the entire time samples were being processed. Despite these efforts to generate reliable and interpretable data, the approach only was applied to KOMP lines with architectural outliers and does not identify patterns that represent a successful compensation to maintain a normal bone structure and function. Inclusion of serum markers of collagen-derived degradation peptides or enhanced collagen formation could be included to identify other candidate KOMP lines for analysis or to interpret KOMP lines with ineffective osteoclast or osteoblast function. An additional problem is the inherent low BV/TV of the trabecular bone in the femur of the C57BL/6NJ line, which increases the variance of the bone surface measurements. Thus, features that were less obvious in the femur were more apparent in the vertebral bone because there is more bone surface to analyze. Going forward, algorithms for assessing cortical bone in either longitudinal sections of the femur or transverse sections of the mid tibia are being developed to provide a histological analysis of the endocortical and periosteal determinants of the cortical bone. Mapping the Raman spectrometry signals of cortical and trabecular bone is an additional step that could be applied to selected KOMP lines to further define the skeletal phenotype.

Presentation and Interpretation of the Knockout Mouse Project Lines

A major effort was expended to develop effective web-based tools to assist the user to identify KOMP lines of interest and to present the screening information in a convincing and interpretable manner. The entry screen of the database portion of the web portal allows the user to search for KOMP lines with a specific architectural or somatic variance, and subsequent graphics are used to illustrate the histomorphometric findings. Behind these graphics is the primary data by group, individual animal, and even individual μCT image or histological section. The goal is to make the data component transparent to the user and even available for downloading for independent data calculations.

The initial search for a low or high total bone volume phenotype returns a large number of responses that can be overwhelming due to the number and dimorphic complexity of the findings. However, the initial list has the advantage that it places the severity of a known skeletal mutation relative to other genes affecting bone mass. This gene effect scale may become important when assessing the composite outcome when multiple skeletal genes are present in the same individual. The screen also reveals almost twice as many HBM lines as LBM. This may reflect that as the LBM phenotype becomes more severe, it becomes a homozygous embryonic lethal that can only be identified by screening heterozygous KOMP lines. In contrast, the HBM should not be a lethal phenotype except in the most extreme cases of osteopetrosis.

To assist the user to develop subgroups of lines with a common phenotype, the search page was designed to perform an AND query to include or exclude a specific measurement in the screening process. From the selection capability, the beginning elements of a classification schema have been initiated. In the classification of LBM, there are three architectural subdivisions in which the low BV/TV phenotype occurs independent or in association with a low bone size or body weight and those with a normal BV/TV but a low bone size and body weight. The underlying assumption is that genes that affect the trabecular bone only are more likely to be bone restricted, while those affecting trabecular, cortical, and body size are genes having a more systemic effect or at least affecting skeletal muscle that secondarily influences the mineralized skeleton [48–50]. The latter category may contain genes, which contribute to a frailty phenotype that is manifested at the time of maximal somatic development and would be predicted to be most susceptible to degenerative changes to the musculoskeletal system with aging. The group with HBM and large bone and body weight may represent a fitness phenotype [51]. GWAS studies imply that genes contributing to frailty and fitness can be identified [52, 53], and these subgroups of mice may be helpful in understanding the importance and mechanism of this degenerative process. As more KOMP lines are examined, it is likely that the classification will expand to identify subgroups that are restricted to dimorphism of sex and gender as well as the basis for the altered body weight as determined by total body NMR which is more sensitive to body and bone marrow fat, muscle, and body water compartments than the DXA tool [54].

Within the LBM group, four classifications based on histological features emerged although more are anticipated as more KOMP lines are examined. Most distinctive is a high turnover/low bone mass phenotype [55] in which the activated osteoblastic lineage is unable to compensate for the high bone resorptive state of the osteoclastic lineage. The basis for the high osteoclast activity can be inherent to the molecular regulation of the osteoclast as in the case of the *Irl8* gene to dysregulation of immune cell production of Rankl or defects in the quality of the bone matrix as found in osteogenesis imperfecta. The other example of an activated osteogenic lineage was found in the *Cp* line, but it differed from high turnover in that the bone formation rate was low and the osteoclast lineage was not activated. The mechanism may be inherent to the osteoblast lineage possibly affecting incomplete differentiation but without producing a defective matrix that activates the osteoclast lineage. The other two categories have the primary feature of low bone formation and relatively dormant osteogenic lineage. The most populated group has features of an adynamic bone in which neither the osteoblast nor osteoclast lineage is activated, and the number of bone remodeling units is extremely low [56, 57]. The other classification demonstrates an activated osteoclastic lineage with a high number of remodeling units, yet an osteogenic response is lacking. This uncoupling effect is likely to have multiple causes arising in either lineage or from an external source [58–60].

The same reasoning for classification can be applied to the HBM group that is formulated on the basis of modeling or remodeling aspects of bone mass accumulation. The most populated group has a state of low remodeling in which bone formation, osteoblast and osteoclast activation, and remodeling units are low, yet bone mass is high. The mechanisms could be an impediment to the expansion of osteoclast lineage [61] or a deficiency of coupling of the osteoblast to the osteoclast lineage [38]. Two previously unappreciated bone-related genes, *R3hcc1* and *Fam186b*, top the list in this category as having the highest BV/TV measurement. The second grouping that also results in low remodeling occurs in the presence of an activated osteoclast lineage with high remodeling units. Because this activated state does not result in a low bone mass phenotype, we assume that a defect in osteoclast function must be present. The appearance of the *Ocstamp* line into this category supports this interpretation, but these histological features need to be confirmed by measuring the serum or excretion levels of collagen degradation peptides. The third group was defined by the *Rin3* line as having continued bone modeling in the absence of a remodeling response. This pattern resembles the histological phenotype of the well-studied high bone mass *LRP5* G171V mutation [62, 63].

The groupings are based on cellular processes as an example of how classification might direct a subsequent investigation of a KOMP line. Note that neither the frailty nor fitness group fit into a single histological category. Clearly, the segmenting rules that were selected here could be organized in a different manner such that a molecular pathway or cell autonomous–cell non-autonomous mechanism of action might be developed for a focus directed at either a genetic or pharmacologic treatment strategy.

Improvements to the Screening and Evaluation Platform

Currently, there are bone phenotyping centers in England, Germany, Austria, Australia, South Korea, and the USA. Given the expected number of IMPC lines that will eventually be produced, this number of centers is well justified. However, each site has a different screening strategy, which precludes developing a unified web portal to report and interpret their findings. Finding a way to provide consistency in the screening and analysis has to be developed either by using similar instruments and protocols and/or by distributing tissues to specific groups that perform one or more of the specialized tests discussed above. Furthermore, a mechanism needs to be developed that notifies specific research groups that an IMPC line has been identified that fits their area of interest and to ship breeders to them to facilitate their further evaluation of the line. Expansion of the phenotype to include craniofacial and dental features would be amenable to the μCT platform while histological characterization of articular and growth plate cartilage could be included into the bone histological workflow. The study of heterozygous IMPC mouse lines that generate late embryonic or neonatal lethal offspring are most likely to have defects in skeletal genes with significant architectural and somatic variation. In fact, they are likely to have a greater gene effect than the heterozygous mice derived from the homozygous lines examined by us to date. Including the variable of aging and other comorbidities must also be factored into the assessment. The fundamental point of the screen and analysis steps is that the IMPC is providing a once-in-a-life time opportunity for studying functional genomics, and the skeletal biology community needs to take advantage of this resource.

Compliance with Ethical Standards

Conflict of Interest David Rowe, Seung-Hyun Hong, Caibin Zhang, Dong-Guk Shin, Renata Rydzik, Li Chen, Zhihua Wu, Gaven Garland, Dana Godfrey, and John Sundberg declare no conflict of interest. Cheryl Ackert-Bicknell reports grants from National Institutes of Health/NIAMS during the conduct of the study. Douglas Adams reports grants from National Institutes of Health.

Human and Animal Rights and Informed Consent This article does not contain any studies with human or animal subjects performed by any of the authors.

References

Papers of particular interest, published recently, have been highlighted as:
- Of importance

1. Weinstein, S.L. and E.H. Yelin. *The Burden of Musculoskeletal Diseases in the United States (BMUS)*. United States Bone and Joint Initiative 2014 [cited 2014; Third Edition:[Available from: http://www.boneandjointburden.org/2014-report/if0/health-care-utilization-and-economic-cost.
2. Jacobs, J.J., et al., *Beyond the decade: strategic priorities to reduce the burden of musculoskeletal disease.* J Bone Joint Surg Am, 2013. **95**(17): p. e1251–6. 3748998.
3. • Alonso N, Ralston SH. *Unveiling the mysteries of the genetics of osteoporosis*. J Endocrinol invest. 2014;**37**(10):925–34. **Until reference 4 is published, this is the most recent overview of the clinical linkage studies that identify gentic loci that impact skeletal variation. The goal is to associate the GWAS studies in humans to the KOMP data in mice.**
4. Kemp J, M. J, Gregson C, Tobias J, Forgetta V, Medina-Gomez MC, et al. *Genome-wide* association study of bone mineral density in the UK Biobank study identifies over 376 loci associated with osteoporosis. Nat Genet. 2017. **in press**;**49**:**1468**–75.
5. McCarthy EF. Genetic diseases of bones and joints. Semin Diagn Pathol. 2011;28(1):26–36.
6. Bonafe L, Cormier-Daire V, Hall C, Lachman R, Mortier G, Mundlos S, et al. Nosology and classification of genetic skeletal disorders: 2015 revision. Am J Med Genet A. 2015;167A(12): 2869–92.
7. Qaseem A, Forciea MA, McLean RM, Denberg TD, for the Clinical Guidelines Committee of the American College of Physicians. Treatment of low bone density or osteoporosis to prevent fractures in men and women: a clinical practice guideline update from the American College of Physicians. Ann Intern Med. 2017;166(11): 818–39.
8. Metcalf LM, Aspray TJ, McCloskey EV. The effects of parathyroid hormone peptides on the peripheral skeleton of postmenopausal women. A systematic review. Bone. 2017;99:39–46.
9. Tashjian AH Jr, Gagel RF. *Teriparatide [human PTH(1-34)]: 2.5 years of experience on the use and safety of the drug for the treatment of osteoporosis*. J Bone Miner Res. 2006;21(3):354–65.
10. Lopez-Delgado L, Riancho-Zarrabeitia L, Riancho JA. Genetic and acquired factors influencing the effectiveness and toxicity of drug therapy in osteoporosis. Expert Opin Drug Metab Toxicol. 2016;12(4):389–98.
11. Rivadeneira F, Makitie O. Osteoporosis and bone mass disorders: from gene pathways to treatments. Trends Endocrinol Metab. 2016;27(5):262–81.
12. Brommage R, et al. *High-throughput screening of mouse gene knockouts identifies established and novel skeletal phenotypes*. Bone Res. 2014;(**2**):14034–40. 4472125
13. Tang T, Li L, Tang J, Li Y, Lin WY, Martin F, et al. A mouse knockout library for secreted and transmembrane proteins. Nat Biotechnol. 2010;28(7):749–55.
14. White JK, Gerdin AK, Karp NA, Ryder E, Buljan M, Bussell JN, et al. Genome-wide generation and systematic phenotyping of knockout mice reveals new roles for many genes. Cell. 2013;154(2):452–64.
15. Brommage R. Genetic approaches to identifying novel osteoporosis drug targets. J Cell Biochem. 2015;116(10):2139–45.
16. • Freudenthal B, et al. *Rapid phenotyping of knockout mice to identify genetic determinants of bone strength*. J Endocrinol. 2016;**231**(1): R31–46. **This is the most recent overview of the various IMPC-relatd bone phenotyping programs with particular emphasis on the mechanical and structural aspects of bone.**
17. • Meehan TF, et al. *Disease model discovery from 3,328 gene knockouts by The International Mouse Phenotyping Consortium*. Nat Genet. 2017;**49**(8):1231–8. **This is the most recent update of the IMPC screening activity. There is no mention of skeletal disorders in the screen, which emphasizes the need for a bone-focused component to this international project.**
18. Bouxsein ML, Uchiyama T, Rosen CJ, Shultz KL, Donahue LR, Turner CH, et al. Mapping quantitative trait loci for vertebral trabecular bone volume fraction and microarchitecture in mice. J Bone Miner Res. 2004;19(4):587–99.
19. Adams DJ, Ackert-Bicknell CL. Genetic regulation of bone strength: a review of animal model studies. Bonekey Rep. 2015;4:714.
20. Hong SH, et al. *Computer-automated static, dynamic and cellular bone histomorphometry*. J Tissue Sci Eng. 2012;(Suppl 1):004.
21. Dyment NA, Jiang X, Chen L, Hong SH, Adams DJ, Ackert-Bicknell C, et al. High-throughput, multi-image cryohistology of mineralized tissues. J Vis Exp. 2016;(115)
22. Kalajzic I, Braut A, Guo D, Jiang X, Kronenberg MS, Mina M, et al. Dentin matrix protein 1 expression during osteoblastic differentiation, generation of an osteocyte GFP-transgene. Bone. 2004;35(1):74–82.
23. Kalajzic I, Staal A, Yang WP, Wu Y, Johnson SE, Feyen JHM, et al. Expression profile of osteoblast lineage at defined stages of differentiation. J Biol Chem. 2005;280(26):24618–26.
24. Parfitt AM, Mundy GR, Roodman GD, Hughes DE, Boyce BF. A new model for the regulation of bone resorption, with particular reference to the effects of bisphosphonates. J Bone Miner Res. 1996;11(2):150–9.
25. Sims NA, Martin TJ. Coupling the activities of bone formation and resorption: a multitude of signals within the basic multicellular unit. Bonekey Rep. 2014;3:481.
26. Fisher RA. On the interpretation of $\chi 2$ from contingency tables, and the calculation of P. J R Stat Soc. 1922;85:87.
27. Kurbatova N, Mason JC, Morgan H, Meehan TF, Karp NA. PhenStat: a tool kit for standardized analysis of high throughput phenotypic data. PLoS One. 2015;10(7):e0131274.
28. Zhao B, Takami M, Yamada A, Wang X, Koga T, Hu X, et al. Interferon regulatory factor-8 regulates bone metabolism by suppressing osteoclastogenesis. Nat Med. 2009;15(9):1066–71.
29. Sims NA, Quinn JM. Osteoimmunology: oncostatin M as a pleiotropic regulator of bone formation and resorption in health and disease. Bonekey Rep. 2014;3:527.
30. Yoshitake H, Rittling SR, Denhardt DT, Noda M. Osteopontin-deficient mice are resistant to ovariectomy-induced bone resorption. Proc Natl Acad Sci U S A. 1999;96(14):8156–60.
31. Zarjou A, Jeney V, Arosio P, Poli M, Zavaczki E, Balla G, et al. Ferritin ferroxidase activity: a potent inhibitor of osteogenesis. J Bone Miner Res. 2010;25(1):164–72.
32. Wiren KM, Toombs AR, Zhang XW. Androgen inhibition of MAP kinase pathway and Elk-1 activation in proliferating osteoblasts. J Mol Endocrinol. 2004;32(1):209–26.
33. Carroll SH, Wigner NA, Kulkarni N, Johnston-Cox H, Gerstenfeld LC, Ravid K. A2B adenosine receptor promotes mesenchymal stem cell differentiation to osteoblasts and bone formation in vivo. J Biol Chem. 2012;287(19):15718–27.
34. Abdelmagid SM, Belcher JY, Moussa FM, Lababidi SL, Sondag GR, Novak KM, et al. Mutation in osteoactivin decreases bone formation in vivo and osteoblast differentiation in vitro. Am J Pathol. 2014;184(3):697–713.
35. Abubaker J, Tiss A, Abu-Farha M, al-Ghimlas F, al-Khairi I, Baturcam E, et al. DNAJB3/HSP-40 cochaperone is downregulated in obese humans and is restored by physical exercise. PLoS One. 2013;8(7):e69217.

36. Pantel J, Legendre M, Nivot S, Morisset S, Vie-Luton MP, le Bouc Y, et al. Recessive isolated growth hormone deficiency and mutations in the ghrelin receptor. J Clin Endocrinol Metab. 2009;94(11):4334–41.
37. Chen Z, Su L, Xu Q, Katz J, Michalek SM, Fan M, et al. IL-1R/TLR2 through MyD88 divergently modulates Osteoclastogenesis through regulation of nuclear factor of activated T cells c1 (NFATc1) and B lymphocyte-induced maturation protein-1 (Blimp1). J Biol Chem. 2015;290(50):30163–74.
38. Henriksen K, Bollerslev J, Everts V, Karsdal MA. Osteoclast activity and subtypes as a function of physiology and pathology—implications for future treatments of osteoporosis. Endocr Rev. 2011;32(1):31–63.
39. Witwicka H, Hwang SY, Reyes-Gutierrez P, Jia H, Odgren PE, Donahue LR, et al. Studies of OC-STAMP in osteoclast fusion: a new knockout mouse model, rescue of cell fusion, and transmembrane topology. PLoS One. 2015;10(6):e0128275.
40. Vallet M, Soares DC, Wani S, Sophocleous A, Warner J, Salter DM, et al. Targeted sequencing of the Paget's disease associated 14q32 locus identifies several missense coding variants in RIN3 that predispose to Paget's disease of bone. Hum Mol Genet. 2015;24(11):3286–95.
41. Kemp JP, Medina-Gomez C, Estrada K, St Pourcain B, Heppe DHM, Warrington NM, et al. Phenotypic dissection of bone mineral density reveals skeletal site specificity and facilitates the identification of novel loci in the genetic regulation of bone mass attainment. PLoS Genet. 2014;10(6):e1004423.
42. Albagha OM, et al. Genome-wide association identifies three new susceptibility loci for Paget's disease of bone. Nat Genet. 2011;43(7):685–9.
43.• Adams DJ, Rowe DW, Ackert-Bicknell CL. *Genetics of aging bone*. Mamm Genome. 2016;**27**(7–8):367–80. **Besides providing the bone phenotypic changes with aging, the paper provides a concise comparison of the BMD measurement by DXA and cortical bone measurement by μCT.**
44. Charles JF, Ermann J, Aliprantis AO. The intestinal microbiome and skeletal fitness: connecting bugs and bones. Clin Immunol. 2015;159(2):163–9.
45. Yan J, Charles JF. Gut microbiome and bone: to build, destroy, or both? Curr Osteoporos Rep. 2017;15:376–84.
46. Guss JD, Horsfield MW, Fontenele FF, Sandoval TN, Luna M, Apoorva F, et al. Alterations to the gut microbiome impair bone strength and tissue material properties. J Bone Miner Res. 2017;32(6):1343–53.
47. Bassett JH, et al. Rapid-throughput skeletal phenotyping of 100 knockout mice identifies 9 new genes that determine bone strength. PLoS Genet. 2012;8(8):e1002858.
48. Migliaccio S, Greco EA, Wannenes F, Donini LM, Lenzi A. Adipose, bone and muscle tissues as new endocrine organs: role of reciprocal regulation for osteoporosis and obesity development. Horm Mol Biol Clin Investig. 2014;17(1):39–51.
49. Urano T, Inoue S. Recent genetic discoveries in osteoporosis, sarcopenia and obesity. Endocr J. 2015;62(6):475–84.
50. Liu P, Ji Y, Yuen T, Rendina-Ruedy E, DeMambro VE, Dhawan S, et al. Blocking FSH induces thermogenic adipose tissue and reduces body fat. Nature. 2017;546(7656):107–12.
51. Morin S, Leslie WD, Manitoba Bone Density P. High bone mineral density is associated with high body mass index. Osteoporos Int. 2009;20(7):1267–71.
52. Young AC, et al. The identification of hereditary and environmental determinants of frailty in a cohort of UK twins. Twin Res Hum Genet. 2016;19(6):600–9.
53. Erusalimsky JD, Grillari J, Grune T, Jansen-Duerr P, Lippi G, Sinclair AJ, et al. In search of 'omics'-based biomarkers to predict risk of frailty and its consequences in older individuals: the FRAILOMIC initiative. Gerontology. 2016;62(2):182–90.
54. Taicher GZ, Tinsley FC, Reiderman A, Heiman ML. Quantitative magnetic resonance (QMR) method for bone and whole-body-composition analysis. Anal Bioanal Chem. 2003;377(6):990–1002.
55. Ravn P, Fledelius C, Rosenquist C, Overgaard K, Christiansen C. High bone turnover is associated with low bone mass in both pre- and postmenopausal women. Bone. 1996;19(3):291–8.
56. Ng AH, Willett TL, Alman BA, Grynpas MD. Development, validation and characterization of a novel mouse model of adynamic bone disease (ABD). Bone. 2014;68:57–66.
57. Massy Z, Drueke T. Adynamic bone disease is a predominant bone pattern in early stages of chronic kidney disease. J Nephrol. 2017;30:629–34.
58. Sims NA, Martin TJ. Coupling signals between the osteoclast and osteoblast: how are messages transmitted between these temporary visitors to the bone surface? Front Endocrinol (Lausanne). 2015;6:41.
59. Delaisse JM. The reversal phase of the bone-remodeling cycle: cellular prerequisites for coupling resorption and formation. Bonekey Rep. 2014;3:561.
60. Andersen TL, Hauge EM, Rolighed L, Bollerslev J, Kjærsgaard-Andersen P, Delaisse JM. Correlation between absence of bone remodeling compartment canopies, reversal phase arrest, and deficient bone formation in post-menopausal osteoporosis. Am J Pathol. 2014;184(4):1142–51.
61. Pacheco-Costa R, Hassan I, Reginato RD, Davis HM, Bruzzaniti A, Allen MR, et al. High bone mass in mice lacking Cx37 because of defective osteoclast differentiation. J Biol Chem. 2014;289(12):8508–20.
62. Little RD, Folz C, Manning SP, Swain PM, Zhao SC, Eustace B, et al. A mutation in the LDL receptor-related protein 5 gene results in the autosomal dominant high-bone-mass trait. Am J Hum Genet. 2002;70(1):11–9.
63. Babij P, Zhao W, Small C, Kharode Y, Yaworsky PJ, Bouxsein ML, et al. High bone mass in mice expressing a mutant LRP5 gene. J Bone Miner Res. 2003;18(6):960–74.